Article:

Efficient use of space-time clustering for underwater acoustic communications

Jianghui Li, *Student Member, IEEE,* and Yuriy Zakharov, *Senior Member, IEEE*

Abstract

Underwater acoustic (UWA) communication channels are characterized by the spreading of received signals in space (direction of arrival) and in time (delay). The spread is often limited to a small number of space-time clusters. In this paper, the space-time clustering is exploited in a proposed receiver designed for guard-free orthogonal frequency-division multiplexing (OFDM) with superimposed data and pilot signals. For separation of space clusters, the receiver utilizes a vertical linear array (VLA) of hydrophones, whereas for combining delay-spread signals within a space cluster, a time-domain equalizer is used. We compare a number of space-time processing techniques, including a proposed reduced-complexity spatial filter, and show that techniques exploiting the space-time clustering demonstrate an improved detection performance. The comparison is done using signals transmitted by a moving transducer, and recorded on a 14-element non-uniform VLA in sea trials at distances of 46 km and 105 km.

Index Terms

OFDM, spatial filter, underwater acoustic communications, vertical linear array

I. Introduction

In underwater acoustic (UWA) communication channels, received signals are spread in angle and delay of arrival [1]. In many communication scenarios, e.g., in deep-water channels, the spreading is concentrated around a few specific directions of arrival (DoA) and delays [2]–[6]. We refer to this phenomenon as space-time clustering, and exploit it to improve the detection performance and reduce the complexity of a receiver. The receiver that we consider here utilizes a vertical linear array (VLA) of hydrophones.

To improve the detection performance, an efficient way is to combine signals from multiple diversity branches [7], e.g., from the antenna array elements. The joint spatial diversity and equalization when applied directly to signals at the antenna elements can provide significant improvement in the performance compared to the single-branch detection [5], [8]–[11]. However, such combining requires a large number of parameters to be estimated, thus often resulting in numerical instability [12]. Moreover, with combining applied directly to antenna elements, a large number of elements is required to achieve a good bit error rate (BER) performance in scenarios with a low signal-to-noise ratio (SNR). In such receivers, the complexity can be high as it is proportional to the number of antenna elements [13]. A more numerically stable and computationally efficient approach

Jianghui Li and Yuriy Zakharov are with the Department of Electronics, University of York, UK, e-mail: jl1384@york.ac.uk, yury.zakharov@york.ac.uk. Preliminary results were reported at the IEEE Oceans-2016 conference in Shanghai, China.

is based on separating the spatial and temporal processing [1], [13]–[15]. Such a separation can be based on coherent path beamforming [14]–[16], which however is computationally demanding due to the eigenvalue decomposition; time-reversal beamforming [3], only applicable to specific communication scenarios; or DoA diversity [2], [4], [17].

The space-time clusters introduce a natural diversity, which can be used to improve the detection performance and reduce the complexity. In order to exploit this opportunity the clusters need to be identified, which requires estimation of the spatial signal distribution [1], [2], [18]. Spatial filters (SFs) estimate the spatial signal distribution. From this, single or multiple directions are chosen for diversity combining [2]–[4]. If directions for further processing are chosen based on the maximum power of arrived spatial signals, several directions from the same space cluster can be chosen, which limits the receiver performance due to correlation of the diversity branches. To achieve a high performance when processing wideband communication signals, a SF would combine properly delayed signals from antenna elements. This requires delays to be fractional with respect to the sampling interval, and a specific set of delays applied for every DoA of interest. As a result, such SFs possess a high complexity [2].

In UWA communications, multi-antenna receivers with diversity combining are used for detection of single carrier [1], [5], [11], [15] and multicarrier [2], [19]–[21] signals. In this paper, we investigate the space-time processing of multicarrier orthogonal frequency-division multiplexing (OFDM) signals. Multi-antenna detection of OFDM signals with cyclic prefix were investigated in [21]. The use of OFDM signals with guard intervals, such as the cyclic prefix, results in a reduced spectral efficiency of communication systems. Higher spectral efficiency is achieved in multicarrier systems with guard-free OFDM signals [22]–[25].

In this paper, we investigate UWA communication with guard-free OFDM signals. In the receiver, a SF computes a spatial signal distribution to estimate DoAs, and further uses these estimates in beamformers to form space diversity branches. We propose a SF that does not require delaying the signals from antenna elements and therefore it is of reduced-complexity compared to the SF with fractional delays. In every diversity branch, an equalizer compensates for the Doppler effect and performs the multipath combining. Finally, the equalized signals from the diversity branches are combined using maximal ratio combining (MRC) [7], demodulated and decoded.

We investigate the performance of the receiver with various space-time processing techniques, and find that the receiver exploiting the space-time clustering demonstrates an improved performance and reduced complexity. The investigation is based on processing signals recorded on a 14-element VLA in sea trials at distances of 46 km and 105 km, with a transducer moved at a speed of 6 m/s. In these two scenarios, when exploiting the space-time clustering, error-free data transmission is achieved with spectral efficiencies of 0.167 bps/Hz and 0.33 bps/Hz, respectively.

This paper is organised as follows. Examples of space-time clusters from sea trials at distances from 30 km to 110 km are presented in Section II. Section III describes the transmitted signal and channel model. Section IV presents space-time processing techniques in the receiver, and Section V compares these techniques. Section VI completes the paper with concluding remarks.

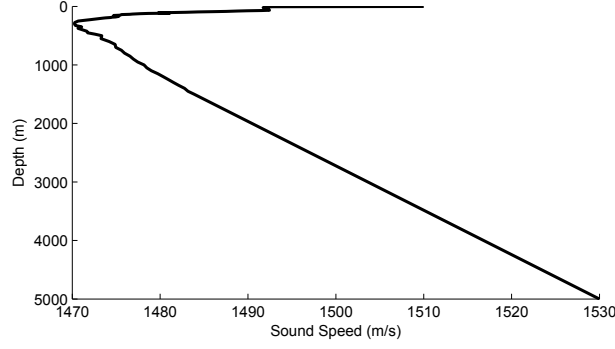## II. Space-time clusters in UWA channels

Fig. 1. The sound speed profile in the sea trials.

In this section, we show examples of space-time clusters observed in sea trials at distances from 30 km to 110 km. The acoustic environment is characterised by the sound speed profile shown in Fig. 1. The sea depth is about 5 km, and the minimum sound speed is at a depth of about 300 m. In the trials, communication signals are transmitted in the frequency band 2560-3584 Hz; a transducer is towed at a depth of around 250 m and a receive VLA of 14 hydrophones is placed at a depth of around 420 m. Fig. 2 shows the hydrophone positions within the VLA of a total length of 8.1 m; the distance between hydrophones varies from 0.3 m to 1.2 m.

Space-time distributions of received signals are shown in Figs. 3(a)-3(l) for various distances between the transmit and receive antennas. It can be seen that in all the cases, the signal distributions are characterised by several peaks representing what we call space-time clusters. These clusters can provide natural diversity branches in a receiver.

When describing the receiver below, for illustration, we will be using the experimental data obtained at a distance of 105 km, see Fig. 3(i).
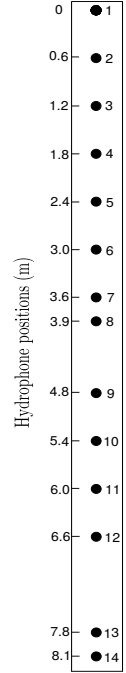

Fig. 2. VLA of 14 hydrophones (circles), and their positions.

III. TRANSMITTED SIGNAL AND CHANNEL MODEL

The transmitted signal $s(t)$ consists of L guard-free OFDM symbols with superimposed data and pilot signals [25], each OFDM symbol given by:

$$s_l(t) = \Re\left\{ e^{j2\pi f_c t} \sum_{k=-N_s/2}^{N_s/2-1} [M_p(k) + jD_l(k)]e^{j\frac{2\pi}{T_s}kt} \right\}, \tag{1}$$

where $\Re\{\cdot\}$ denotes the real part of a complex number, $N_s = 1024$ the number of sub-carriers, $f_c = 3072$ Hz the carrier frequency, $T_s = 1$ s the OFDM symbol duration, and $j = \sqrt{-1}$. The sequence $M_p(k) \in [-1, +1]$ is a binary pseudo-random sequence of length N_s, serving as the pilot signal. The binary sequence $D_l(k)$ represents the information data in the lth OFDM symbol, $l = 1, \ldots, L$; it is obtained by encoding and interleaving the original data across sub-carriers using convolutional codes [26]. Specific codes used with the experimental data will be clarified in Section V.

The UWA channel is often modelled as a time-variant linear system with an impulse response $h_m(t, \tau)$ that describes

(a) 30 km

(b) 39 km

(c) 46 km

(d) 50 km

(e) 94 km

(f) 100 km

(g) 102 km

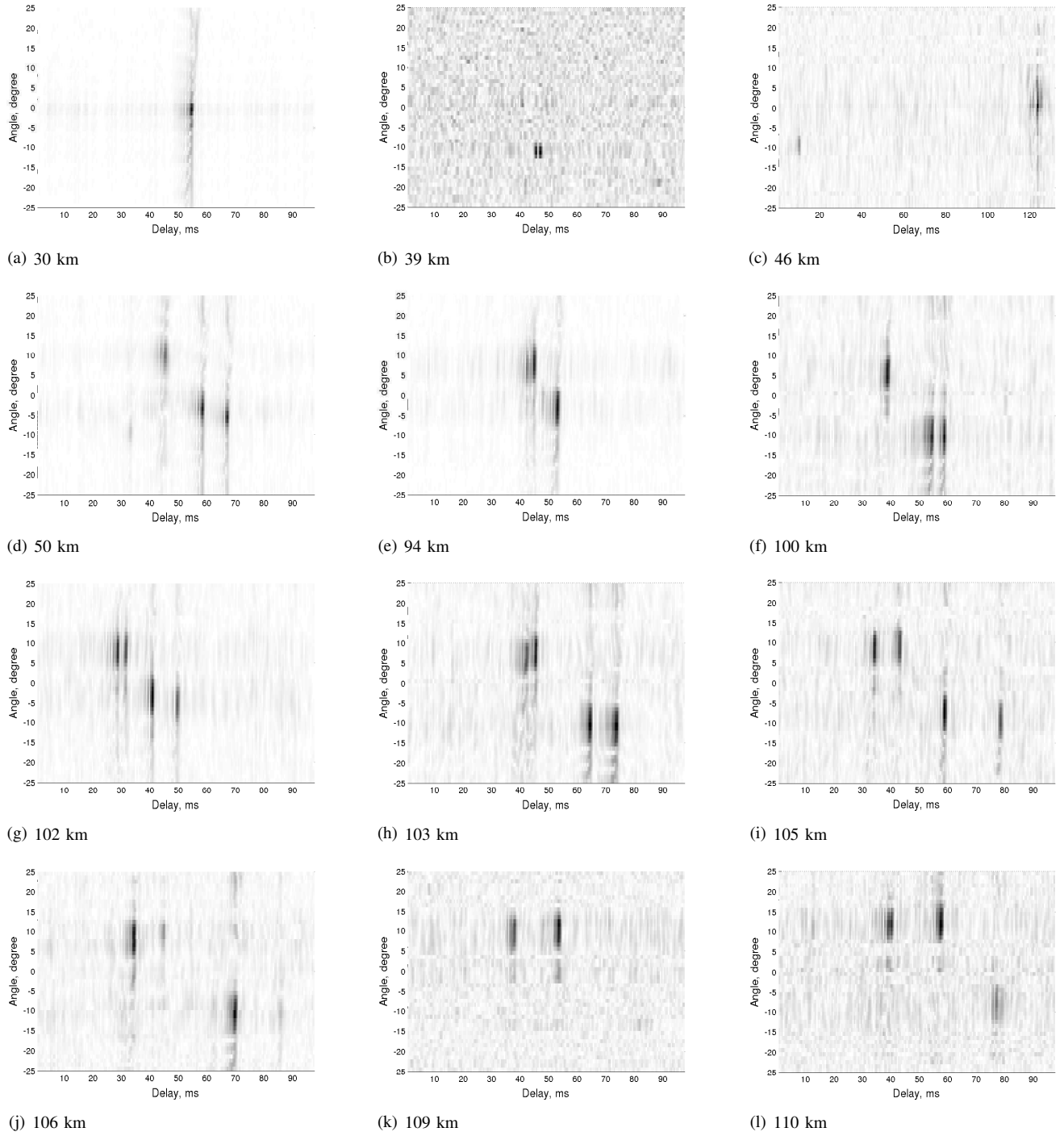(h) 103 km

(i) 105 km

(j) 106 km

(k) 109 km

(l) 110 km

Fig. 3. Experimental space-time distributions of received signal observed at various distances; positive angles correspond to acoustic rays received from the sea surface direction while negative angles show rays from the sea bottom direction.

multipath and Doppler spreads in the channel. The received signal at the m-th hydrophone is then given by

$$\mathrm{r}_m(t) = \int_{-\infty}^{\infty} \mathrm{h}_m(t,\tau)\mathrm{s}(t-\tau)d\tau + \nu_m(t), \quad m = 1, \ldots, M, \tag{2}$$

where M is the number of hydrophones in the VLA, and $\nu_m(t)$ is the additive noise. Various models of $\mathrm{h}_m(t,\tau)$ can be used;

e.g., for a channel with Q discrete multipath components we have [27], [28]:

$$\mathrm{h}_m(t,\tau) = \sum_{q=1}^{Q} A_{q,m}(t)\delta(\tau - \tau_{q,m}(t)), \tag{3}$$

where $A_{q,m}(t)$ is the amplitude of the qth multipath component at the mth hydrophone, and $\delta(t)$ is the Dirac delta function. The time variation of the delay $\tau_{q,m}(t)$ is caused by the Doppler effect; the slope (gradient) of the time dependence defines the time compression experienced by the signal. One of challenges in processing signals received in such a channel, is due to different time compressions of signals received via different multipaths. As a consequence, the simple time compression operation, implemented in practice via resampling the received signal, cannot completely remove the Doppler distortion.

However, multipath components arrived from a particular (jth) direction tend to have close values of the time-compression factor. Therefore, the Doppler distortion in a signal from the jth direction can be accurately compensated for by resampling. After the resampling, the channel can be modelled by an impulse response

$$\tilde{\mathrm{h}}_j(t,\tau) = \sum_{q=1}^{Q_j} A_{q,j}(t)\delta(\tau - \tau_{q,j}), \tag{4}$$

where the delays $\tau_{q,j}$ are now constant and Q_j is the number of multipath components in the jth space branch, $Q_j \leq Q$. The time-invariant property of the path delays allows a higher accuracy of channel estimation/equalization and, eventually, better detection performance of the receiver. A reduced channel delay spread in directional signals also allows a better detection performance and reduced complexity.

Signals received from several directions and equalized can be combined to further improve the detection performance. The performance after the diversity combining will depend on the energy of the received signals, and also on correlation of channels in diversity branches. It is therefore possible that weaker signals from uncorrelated directions after combining, will provide a better detection performance compared to combining strong signals received from correlated directions.

IV. SPACE-TIME PROCESSING IN THE RECEIVER

In this section, we describe the receiver (see Fig. 4). The analog signals received by M hydrophones are bandpass filtered within the frequency band of the OFDM transmission and converted into the digital form $\mathrm{r}_1(i)$ to $\mathrm{r}_M(i)$ at a sampling rate f_s, i being the discrete time index; $f_s = 4f_c = 12288$ Hz in our case. The digital signals $\mathrm{r}_1(i)$ to $\mathrm{r}_M(i)$ are processed in a SF that produces J directional signals $\mathrm{r}(i, \hat{\theta}_j)$, $j = 1, \ldots, J$. The angles $\hat{\theta}_j$ are chosen from the average signal power as a function of DoA. The directional signals are equalized in the time domain, transformed into the frequency domain using the fast Fourier transform (FFT), and combined using the MRC. The combined frequency domain signal $\tilde{\mathrm{X}}_l(k)$ is transferred to a demodulator and, after deinterleaving, further to the soft-decision Viterbi decoder [26].

A. Spatial filters

The following six SFs are considered in this paper:

1) *Single-element SF:* The signal $\mathrm{r}_1(i)$ received at the first hydrophone is the only output of the SF.

2) *Multiple-elements SF:* The M received signals $\mathrm{r}_1(i), \ldots, \mathrm{r}_M(i)$ are M outputs of the SF.
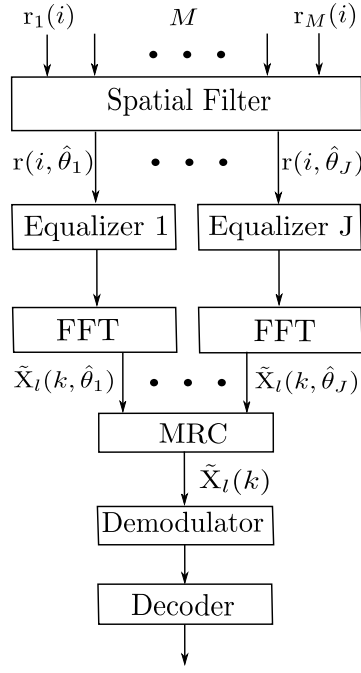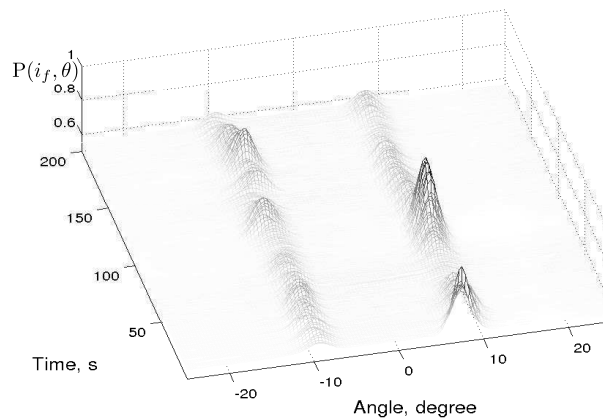
Fig. 4. Block diagram of the receiver.

3) SF with a single direction corresponding to the maximum power of spatial distribution: The time-varying power $\mathrm{P}(i_f; \theta)$ (see Fig. 5, where i_f is the time variable) and the average power $\tilde{\mathrm{P}}(\theta)$ (see Fig. 6) are computed in a DoA estimator (see Fig. 7) as explained below in Section IV-B. Based on the maximum power of the spatial distribution, a single ($J = 1$) direction $\hat{\theta}_1$ is chosen:

$$\hat{\theta}_1 = \arg\max_{\theta} \tilde{\mathrm{P}}(\theta). \tag{5}$$

The beamformer produces a single directional signal $\mathrm{r}(i, \hat{\theta}_1)$.

Fig. 5. Spatial power distribution $\mathrm{P}(i_f; \theta)$ in the experiment at the distance 105 km.
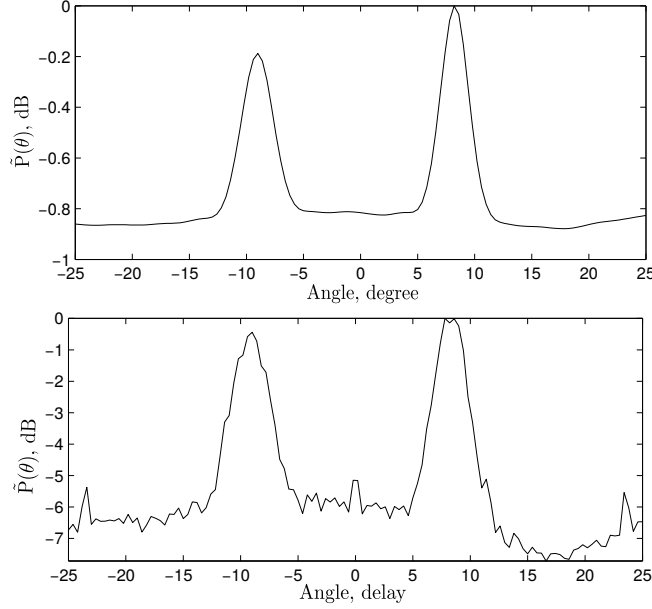
Fig. 6.   The average spatial signal power $\tilde{P}(\theta)$ in the experiment at the distance 105 km, computed in SF 3, SF 4, and SF 5 (with non-fractional delay beamforming) [top] or in SF 6 (with fractional delay beamforming) [bottom].
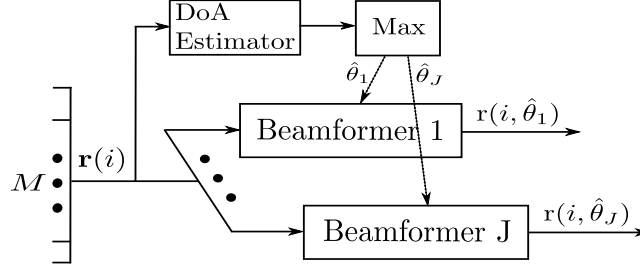

Fig. 7.   Block diagram of the SF with J outputs based on maxima of the spatial signal power.

4) SF with J directions corresponding to J maxima of spatial distribution: In this case (see Fig. 7), several directions ($J \geq 2$) are chosen, corresponding to the first J maxima of the average power distribution $\tilde{P}(\theta)$:

$$[\hat{\theta}_1, \ldots, \hat{\theta}_J] = \arg \max_{\theta} \tilde{P}(\theta). \qquad (6)$$

Note that the function $\tilde{P}(\theta)$ is computed on a grid of angles θ; in our experiments, we use a grid within the interval $\theta \in [-25°, 25°]$ with a step of $0.4°$.

5) SF with J directions corresponding to J space clusters: In this SF that we propose, a peak detector $\mathbb{P}$ finds J local maxima of $\tilde{P}(\theta)$, which are considered to correspond to space clusters. With this technique, two ($J = 2$) space clusters are identified in the experiment at the distance 105 km [see Fig. 3(i)]. The two clusters occupy angle intervals $[6°, 11°]$ and $[-12°, -6°]$, but in each of them, a single angle $\hat{\theta}_j$ ($\hat{\theta}_1 = 8.4°$ and $\hat{\theta}_2 = -9°$, respectively) is chosen for further processing:

$$[\hat{\theta}_1, \ldots, \hat{\theta}_J]^T = \mathbb{P}[\tilde{P}(\theta)]. \qquad (7)$$

6) SF with fractional delays and J directions corresponding to J space clusters: In SFs 3, 4 and 5 described above, low-complexity DoA estimation and beamforming techniques presented below in Section IV-B are used. More accurate but also

more complicated DoA estimation and beamforming are used in the SF with fractional delays. To achieve a high accuracy when processing wideband signals, such as communication signals, both the DoA estimator and beamformer should operate by introducing delays (fractional delays with respect to the sampling interval) in the hydrophone signals. In this fractional delay beamforming technique, the $M \times N$ snapshot matrix $\mathbf{X}(\theta)$ for a specific direction θ is used for calculating the diagonally loaded sample covariance matrix [2]

$$\mathbf{R}(\theta) = \mathbf{X}(\theta)\mathbf{X}^T(\theta) + \kappa \mathbf{I_M}, \tag{8}$$

and

$$[\mathbf{X}(\theta)]_{m,n} = r_m(nT - \varsigma(m,\theta)), \ \ n = 1, 2 \ldots, N, \tag{9}$$

where $(\cdot)^T$ denotes the transpose, $\mathbf{I}_M$ an $M \times M$ identity matrix, and κ a loading factor which is a small positive number used here to prevent numerical instability. In our numerical examples, the value of N is set to the total number of received samples in a communication session. The signal values $r_m(nT - \varsigma(m,\theta))$ in (9) are recovered by interpolation of the digital signal $r_m(i)$ from the mth hydrophone at the time instants $t = nT - \varsigma(m,\theta)$, where $T = 1/f_s$; for this purpose, we use the linear interpolation. The delays are different for each direction θ and computed as

$$\varsigma(m,\theta) = \frac{\mathrm{D}(m)\sin(\theta)}{c}, \tag{10}$$

where $\mathrm{D}(m)$ is the distance between the first ($m = 1$) and mth hydrophone (see Fig. 2) and the sound speed $c = 1500$ m/s. The spatial signal power $\tilde{\mathrm{P}}(\theta)$ is computed according to

$$\tilde{\mathrm{P}}(\theta) = \left[\sum_{m=1}^{M} \sum_{n=1}^{M} [\mathbf{R}^{-1}(\theta)]_{m,n} \right]^{-1}. \tag{11}$$

The beamforming weights for a direction θ are computed as

$$\tilde{\mathrm{w}}(\theta) = \tilde{\mathrm{P}}(\theta) \left[\sum_{n=1}^{M} [\mathbf{R}^{-1}(\theta)]_{1,n}, \ldots, \sum_{n=1}^{M} [\mathbf{R}^{-1}(\theta)]_{M,n} \right]^T. \tag{12}$$

The received signal for a direction $\hat{\theta}_j$ is then computed as

$$\mathrm{r}(i, \hat{\theta}_j) = \left[\mathbf{X}^T(\hat{\theta}_j) \tilde{\mathrm{w}}(\hat{\theta}_j) \right]_i. \tag{13}$$

This beamforming technique uses interpolation and processes each direction separately, making this SF more complicated [2].

B. Low-complexity DoA estimator and beamformer

The DoA estimator computes the spatial power distribution to estimate DoAs, then beamformers, using these DoA estimates, produce directional signals. In this section, we propose simplified DoA estimator and beamformer not requiring the fractional delays.

1) DoA estimator: The DoA estimator computes the spatial power distribution of the received signal by processing the hydrophone signals $\mathrm{r}_1(i)$ to $\mathrm{r}_M(i)$. The ith time domain snapshot of received signals is described as an $M \times 1$ vector

$\mathbf{r}(i) = [\mathrm{r}_1(i), \mathrm{r}_2(i), \ldots, \mathrm{r}_M(i)]^T$. The snapshots are divided into N_f frames of I_f snapshots each. A frame is divided into N_{sf} non-overlapping subframes of U snapshots each, i.e., $I_f = N_{sf}U$. The subframes are transformed into the frequency domain; the $M \times 1$ frequency domain snapshot at frequency ω_k for a subframe starting at time u is given by

$$\mathbf{z}(u;k) = \sum_{n=0}^{U-1} \mathbf{r}(u+n)e^{-j\omega_k n/f_s}, \tag{14}$$

where $k = 0, \ldots, K-1$, $K = 2\pi F/\Delta\omega$, F is the bandwidth of interest, $\omega_k = \omega_0 + k\Delta\omega$, $\Delta\omega = 2\pi f_s/U$, and ω_0 the lowest frequency of interest. For a frame starting at time i_f, for every frequency ω_k, the $M \times M$ covariance matrix is computed as [29]:

$$\mathbf{Y}(i_f;k) = \frac{1}{N_{sf}} \sum_{n_{sf}=0}^{N_{sf}-1} \mathbf{z}(i_f + n_{sf}U;k)\mathbf{z}^H(i_f + n_{sf}U;k) + \kappa\mathbf{I}_M. \tag{15}$$

In our experiments, the loading factor κ was set to a small value to prevent numerical instability when inverting the matrix $\mathbf{Y}(i_f;k)$ (see below). More specifically, it was set to at most 10^{-8} of $(1/M)\mathrm{trace}\{\mathbf{Y}(i_f;k)\}$, where $\mathrm{trace}\{\cdot\}$ is the matrix trace. The loading factor κ can be optimized to achieve an improved detection performance [30]; however, in this paper, we do not consider such optimization. The matrix $\mathbf{Y}(i_f;k)$ is used for obtaining the spatial power at every angle of arrival θ using the minimum variance distortionless response (MVDR) algorithm [31]. For a frequency ω_k, the steering vector is given by

$$\mathbf{v}(\theta,k) = \left[1, \ldots, e^{-j\omega_k \frac{\mathrm{D}(m)\sin(\theta)}{c}}, \ldots, e^{-j\omega_k \frac{\mathrm{D}(M)\sin(\theta)}{c}}\right]^T. \tag{16}$$

The power at frequency ω_k from a direction θ is given by

$$\mathrm{P}_k(i_f;\theta) = \left[\mathbf{v}^H(\theta,k)\mathbf{Y}^{-1}(i_f;k)\mathbf{v}(\theta,k)\right]^{-1}. \tag{17}$$

The total power over all frequencies

$$\mathrm{P}(i_f;\theta) = \sum_{k=0}^{K-1} \mathrm{P}_k(i_f;\theta) \tag{18}$$

is shown in Fig. 5. The average power over N_f frames (shown in Fig. 6) is given by

$$\tilde{\mathrm{P}}(\theta) = \frac{1}{N_f} \sum_{n_f=1}^{N_f} \mathrm{P}(i_f;\theta). \tag{19}$$

2) *Beamformer:* For a chosen direction $\hat{\theta}_j$, for cancelling the interference arriving from the other directions, the beamformer weight vector $\bar{\mathbf{w}}_{n_f}(\hat{\theta}, k)$ in the n_f-th frame is calculated as

$$\bar{\mathbf{w}}_{n_f}(\hat{\theta}_j, k) = \mathbf{Y}^{-1}(i_f;k)\mathbf{v}(\hat{\theta}_j, k)\mathrm{P}_k(i_f;\hat{\theta}_j). \tag{20}$$

The weight vector is then smoothed in time:

$$\mathbf{w}_{n_f}(\hat{\theta}_j, k) \leftarrow \lambda\mathbf{w}_{n_f-1}(\hat{\theta}_j, k) + (1-\lambda)\bar{\mathbf{w}}_{n_f}(\hat{\theta}_j, k), \tag{21}$$

where $0 \leq \lambda < 1$ is a forgetting factor, and $\mathbf{w}_0(\hat{\theta}_j, k) = \bar{\mathbf{w}}_1(\hat{\theta}_j, k)$. Since the DoAs are slowly varying in time (see Fig. 5), the forgetting factor λ can be chosen close to unity, providing a good filtering of the noise and interference; in our experiment, we set $\lambda = 0.998$. The directional signal is then computed as

$$\mathrm{r}(i, \hat{\theta}_j) = \sum_{k=0}^{K-1} \mathbf{w}_{n_f}^H(\hat{\theta}_j, k) \mathbf{z}(u; k) e^{j\omega_k n/f_s}, \tag{22}$$

where $\mathbf{z}(u; k)$ is as defined in (14), $i = u + n$, $u = i_f + n_{sf}U$, and $n = 0, \ldots, U - 1$.

3) Complexity of the proposed SF: For the DoA estimation, the proposed SF requires the time-frequency transform (14), computation of the matrix in (15), and the power computation (17); the complexity of the other processing steps is significantly lower and can be ignored. The complexity of the three steps are given by $2KMf_s$, $4KN_{sf}M^2 f_s/I_f$, and $4(KM^3 + KN_\theta M^2)f_s/I_f$ real-valued multiply-accumulate operations per second (MAC/s), respectively, where N_θ is the number of angles in the DoA grid. In the beamformer, the frequency-time transform (22) needs to be performed; the other operations require significantly lower complexity. This transform requires $(4KMN_{sf}f_s/I_f + 4Kf_s)$ MAC/s; for J beamformers, this should be multiplied by J. For example, with $M = 14$, $K = 32$, $N_{sf} = 32$, $I_f = 12288$, $N_\theta = 126$, $J = 2$, and $f_s = 12288$ Hz, which are the same as these used in the receiver in Section V, the total complexity of the SF is 1.9×10^7 MAC/s. Note that the complexity of the SF with fractional delays [2], with the same parameter values is about 1.3×10^9 MAC/s; thus, in this scenario, the proposed SF is about 70 times less complicated than the SF with fractional delays.

C. Equalizer

Once a directional signal $\mathrm{r}(i, \hat{\theta}_j)$ has been obtained, it is applied to the equalizer shown in Fig. 8, where the signal is down-shifted and lowpass filtered (LPF) to produce the baseband digital signal $\tilde{r}(i, \hat{\theta}_j)$. The signal $\tilde{r}(i, \hat{\theta}_j)$ is resampled to compensate for the Doppler effect and linearly equalized.
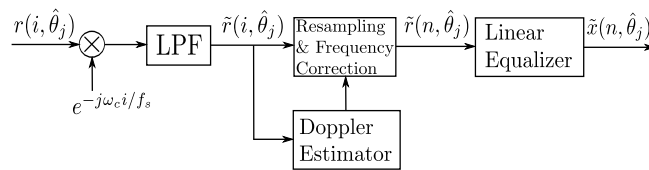

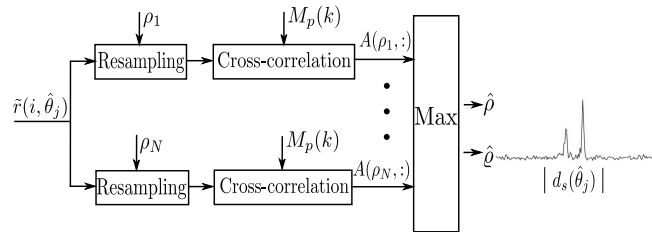Fig. 8. Block diagram of the equalizer.

Fig. 9. Block diagram of the Doppler estimator.

1) Doppler estimator: Fig. 9 shows the block diagram of the Doppler estimator. Techniques for Doppler estimation and compensation can be found in [25], [27], [32]–[37]. In this paper, the cross-ambiguity function method as described in [25] is

used. The time-varying dominant Doppler scale factor and delay are estimated by computing the ambiguity function as follows: firstly, the baseband signal $\tilde{r}(i, \hat{\theta}_j)$ is resampled with a number of compression factors ρ_n, $n = 1, \ldots, N$; then, N Doppler sections of the ambiguity function between the received and pilot signals are computed on the delay-Doppler scale grid [23], [38], [39]. The ambiguity function $A(\rho, \varrho)$ (see [25] for details), where ρ indicates the ρth Doppler section and ϱ indicates the ϱth delay, is used to estimate the dominant Doppler compression and delay:

$$[\hat{\rho}, \hat{\varrho}] = \arg \max_{\rho, \varrho} A(\rho, \varrho). \tag{23}$$

The estimated dominant channel delay is used for the timing synchronization. In a multipath channel, however, there will be a delay spread. Using the $\hat{\rho}$th Doppler section, the Doppler estimator also estimates the delay spread $d_s(\hat{\theta}_j)$ (see Fig. 9). The estimated delay spread is used to set the length of the linear equalizer as explained below in Section V.

2) Linear equalizer: Fig. 10 shows the block diagram of the linear equalizer, which is based on channel estimation and finite impulse response (FIR) filtering [24]. The equalizer length is typically chosen as three to five times the channel delay spread $d_s(\hat{\theta}_j)$ [8], and therefore, if the delay spread is reduced, the equalizer complexity can also be reduced.
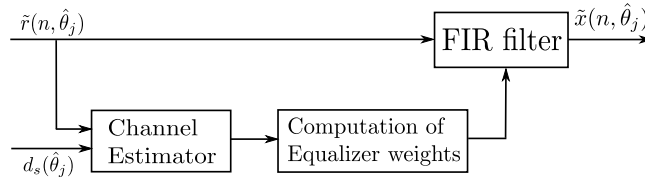

Fig. 10. Block diagram of the linear equalizer.

In the channel estimator, a sparse recursive least square (RLS) adaptive filter (see [24] for more details) is used to estimate the multipath structure of the directional signals. The equalizer weights are computed and interpolated as detailed in [25]. After FIR filtering, the equalized signals $\tilde{x}(n, \hat{\theta}_j)$ from all directions are linearly combined.

D. Diversity combining

The MRC is known to provide the highest SNR in the combined signal [7]. In general, phases of the complex-valued MRC weights should compensate for phase shifts in the directional signals, while the weight magnitudes should be proportional to SNRs in the directional signals. The phase compensation has already been achieved in the equalizer. Therefore, to compute the MRC weights, we only need to estimate SNRs in the equalized directional signals. The SNR estimates can be obtained from the superimposed pilot signal in the frequency domain, since after the equalization the pilot and data sequences are separated.

In the lth symbol of the jth diversity branch, the residual error $e_l(j, k)$ at frequency k is computed as

$$e_l(j, k) = M_p(k) - \Re\{\tilde{X}_l(k; \hat{\theta}_j)\}, \tag{24}$$

where $\Re\{\tilde{X}_l(k; \hat{\theta}_j)\}$ is an estimate of the pilot sequence after the equalization. Since the pilot energy is $\sum_{k=1}^{N_s} |M_p(k)|^2 = N_s$ and the energy of the residual signal is $E_l(j) = \sum_{k=1}^{N_s} |e_l(j, k)|^2$, we adopt the following SNR estimate:

$$\mathrm{SNR}_l(j) = \frac{N_s}{E_l(j)}, \tag{25}$$

where

$$\bar{E}_l(j) = \alpha \bar{E}_{l-1}(j) + (1-\alpha) E_l(j), \ l = 1, 2, \ldots, L, \tag{26}$$

$\bar{E}_0(j) = E_1(j)$, and the forgetting factor $0 \leq \alpha < 1$ is chosen close to unity; in our experiments, $\alpha = 0.99$.

The MRC weight for the l-th OFDM symbol in the j-th diversity branch is then computed as

$$W_l(j) = \frac{\sqrt{\text{SNR}_l(j)}}{\sum_{n=1}^{J} \sqrt{\text{SNR}_l(n)}}, \ l = 1, 2, \cdots, L. \tag{27}$$

The combined signal in the frequency domain is then given by

$$\tilde{X}_l(k) = \sum_{j=1}^{J} W_l(j) \tilde{X}_l(k; \hat{\theta}_j). \tag{28}$$

The sequence $\tilde{X}_l(k)$ is demodulated, deinterleaved, and decoded.

V. EXPERIMENTAL RESULTS

In this section, we compare the BER performance and complexity of the receiver with the six SFs described in Section IV-A, firstly when all diversity branches have the same equalizer lengths, and secondly, with the equalizer lengths adaptively adjusted according to the estimated channel delay spreads.

When processing received signals in the proposed SF, the frame duration is set to 1 s with a number of subframes $N_{sf} = 32$ and number of snapshots in a subframe $U = 384$; $K = 32$ frequencies are processed in the bandwidth of interest, $F = 1024$ Hz, and the lowest frequency of interest is $\omega_0/(2\pi) = 2560$ Hz. The angles θ for DoA estimation are computed in the interval $[-25°, 25°]$ with an angle step of $0.4°$. Experimental results from sea trials at distances of 105 km and 46 km are presented below.

A. Experiment at the distance 105 km

In this sea trial, $L = 200$ guard-free OFDM symbols were continuously transmitted. The space-time clusters for this trial are shown in Fig. 3(i). It can be seen that for each of the two DoAs, at $8.4°$ and $-9°$, there are two macro-paths with different delays. The beamformer is not capable of separating these paths and further equalization is required.

1) Comparison of SFs: In this subsection, results are presented for the case when the RLS filter length in the channel estimator is set to 75 ms, which matches to the channel delay spread at a single hydrophone, while the equalizer length is set to 250 ms. For every OFDM symbol, the transmitted data are encoded using the convolutional code of rate 1/3 with the polynomial [225 331 367] in octal (see [26]).

Fig. 6 shows the spatial distribution of the received signal averaged over the communication session and obtained using either the proposed non-fractional delay beamforming (top plot) or the fractional delay beamforming (bottom plot). The former is used in SF 3, SF 4, and SF 5, whereas the latter is used in SF 6. Since the communication signal is wideband, in general, the fractional-delay SF, combining signals after precise compensation of the hydrophone delays corresponding to a particular

DoA, should provide a better performance. This can be seen if comparing the two plots in Fig. 6, where the fractional-delay technique shows a higher gap (about 5 dB against 0.8 dB) between the peaks indicating the arrived paths and the floor level due to the noise. However, introducing the fractional delays in the signals requires an interpolation that results in a high complexity of SF 6. In the proposed SF 5, the interpolation is not required, and instead, the discrete Fourier transform (DFT) in (14) with weighting (22) specific to DFT bins is used; this operation can efficiently exploit the fast Fourier transform. Therefore, the complexity is significantly reduced. This indeed is achieved with some degradation in the performance as can be seen in Fig. 6. However, as will be seen below, the degradation in the detection performance is very small if any.

Table I compares the BER performance and complexity of the receiver with different SFs. It is seen that the proposed DoA estimator and beamformer (introduced in Section IV-B and used in SFs 3, 4 and 5), reduce the receiver complexity by 8–15 times compared to the receiver with the SF using fractional delays (SF 6). Note that a single equalizer branch requires about 8.3×10^7 MACs (see the complexity analysis in [25] and [40]).

TABLE I
COMPARISON OF RECEIVERS WITH DIFFERENT SPATIAL FILTERS; SEA TRIAL AT THE DISTANCE 105 KM

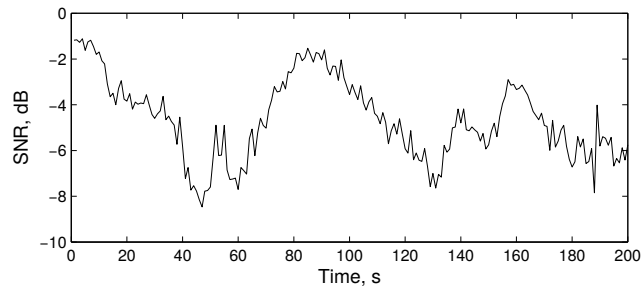| SF	Comments	BER	Complexity (10^6 MAC/s)
1	Single hydrophone	0.45	83
2	All 14 hydrophones	2.7×10^{-3}	1164
3	Single angle $8.4°$	9.1×10^{-2}	100
4	Angles $8.4°$ and $8.8°$	8.9×10^{-2}	185
5	**Cluster ($8.4°$ and $-9°$)**	0	185
6	Cluster ($8.4°$ and $-9°$)	0	1489

Fig. 11. SNR at the first hydrophone in the sea experiment at a distance of 105 km.

From Table I, it is seen that the receiver applied to a single hydrophone (SF 1) is unable to recover reliably the transmitted data. This is due to a low SNR on a single hydrophone, as shown in Fig. 11. The receiver with equalizers applied directly to all 14 antenna elements (SF 2) significantly reduces the BER, but the complexity greatly increases. With one or two diversity branches chosen based on the maxima of the average spatial power distribution (SF 3 and 4, respectively), the BER performance also improves. The difference in the performance between these two SFs is small, but the complexity of the SF with two branches is almost double. With DoAs corresponding to the two space clusters (SF 5), the receiver provides an error-free transmission. Such a receiver has the best performance, and 6.3 times less complexity compared to the receiver with

equalizers applied directly to 14 antenna elements (SF 2). SF 6 (with fractional delays) also allows an error-free transmission with the two branches, but its complexity is significantly higher than that of the receiver with the proposed SF 5.

Note that increasing the number of space diversity branches in SF 4 does allow improvement in the detection performance. With $J = 5$ such branches, an error-free transmission is also achieved. However, the complexity in this case would be 4.4×10^8 MACs, which is about 2.4 times higher than that of the SF 5 with two branches.

2) Equalizer optimization: Fig. 12(a) shows fluctuations of the channel impulse response over the communication session at the first hydrophone; four multipaths can be seen. We now consider two signals from directions $\hat{\theta}_1 = 8.4°$ and $\hat{\theta}_2 = -9°$; fluctuations of channel impulse responses for these directions are shown in Fig. 12(b) and Fig. 12(c), respectively. It can be seen that the four multipaths are now split between the two directions. As a result, the delay spreads in the diversity branches are also reduced compared to that at a single antenna element. We can exploit this to further reduce complexity of the receiver, by setting the channel estimator and equalizer lengths according to the delay spreads of directional signals.

The delay spread of the signal received at the first hydrophone is estimated as about 50 ms. To cover all delay fluctuations throughout the communication session, the RLS filter length is set to 75 taps, with approximately 1 ms/tap; then the equalizer length is set to 250 taps. At angle $\hat{\theta}_1 = 8.4°$, the delay spread $d_s(\hat{\theta}_1)$ is estimated as 12 ms; the RLS filter length is set to 18 taps and the equalizer length is set to 60 taps. At angle $\hat{\theta}_2 = -9°$, the delay spread $d_s(\hat{\theta}_2)$ is estimated as 24 ms; the RLS filter length is set to 36 taps and the equalizer length is set to 120 taps.
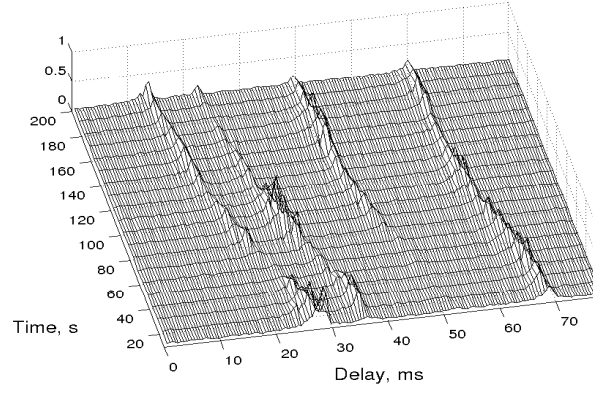
The reduced delay spread in the diversity branches compared to the delay spread at a single hydrophone allows reduction in the receiver complexity. Moreover, the reduced number of channel taps to be estimated also allows a higher estimation accuracy.

Fig. 13(a) shows the Doppler-delay spread of the signal arrived at the first hydrophone. It can be seen that the first and second groups of multipaths are Doppler-shifted with respect to each other. Therefore, the Doppler effect cannot be compensated by resampling the hydrophone signals; there will be a residual Doppler effect seen by the equalizer as fast channel fluctuations. Fig. 13(b) and Fig. 13(c) show the Doppler-delay spread of the two directional signals at angles $\hat{\theta}_1 = 8.4°$ and $\hat{\theta}_2 = -9°$, respectively. It is seen that, compared to Fig. 13(a), Doppler spreads in Fig. 13(b) and Fig. 13(c) are reduced, i.e., the speed of channel variation in the two diversity branches are also reduced, thus allowing a better channel estimation and equalization performance.

TABLE II

PERFORMANCE OF THE RECEIVER WITH OPTIMIZED EQUALIZERS; SEA TRIAL AT THE DISTANCE 105 KM

SF	Equalizer lengths	BER for code polynomials			Complexity
		[5 7 7]	[25 33 37]	[225 331 367]	(10^6 MAC/s)
5	250 ms, 250 ms	3.3×10^{-3}	1.6×10^{-4}	0	185
5	**60 ms, 120 ms**	2.8×10^{-3}	0.8×10^{-4}	0	94
6	250 ms, 250 ms	6.4×10^{-4}	3.9×10^{-4}	0	1489
6	60 ms, 120 ms	4.0×10^{-4}	1.1×10^{-4}	0	1398

Table II shows the BER performance and complexity of the receiver, using SFs 5 and 6, with and without adjusting the equalizer length to the delay spread of directional signals. In the latter case, both the equalizers are of length 250 ms, whereas
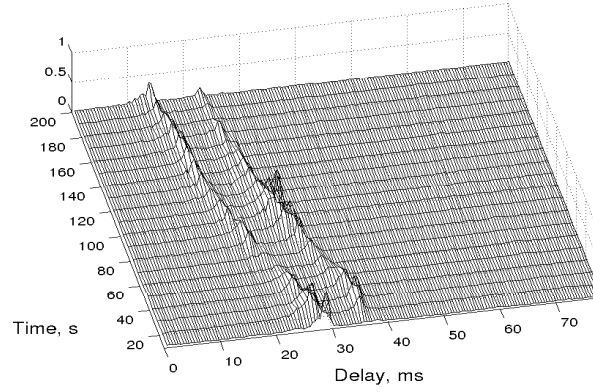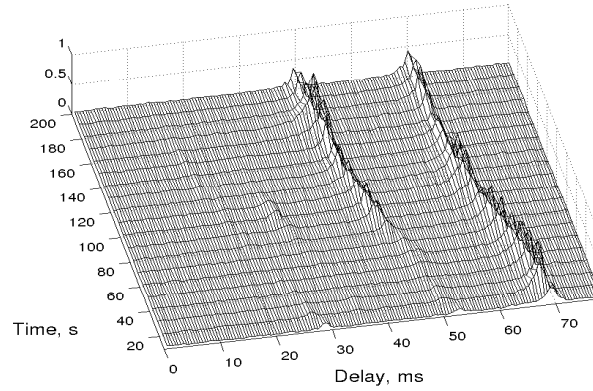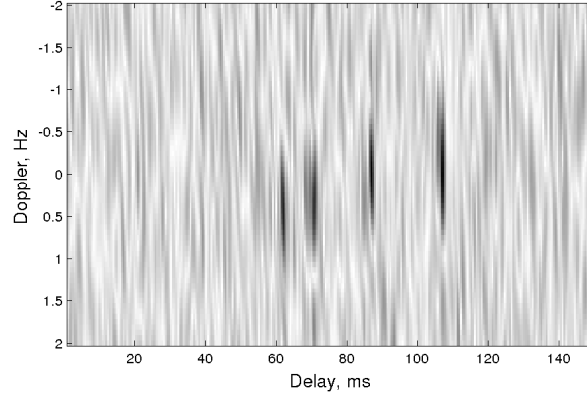
(a) Received signal at the 1st hydrophone.

(b) Directional signal at $\hat{\theta}_1 = 8.4°$.

(c) Directional signal at $\hat{\theta}_2 = -9°$.

Fig. 12. Fluctuations of the channel impulse response in the experiment at the distance 105 km.

in the former case, the equalizer length for the DoA $\hat{\theta}_1 = 8.4°$ is set to 60 ms, and the equalizer length for the DoA $\hat{\theta}_2 = -9°$ is set to 120 ms. It is seen that the shorter equalizers allow reduction in the complexity of the receiver with the proposed SF by about 2 times. This however, is not the case for the receiver with SF 6, since the complexity of SF 6 dominates the receiver complexity.

Results in Table II are presented for three convolutional codes, all codes are of rate 1/3. With the stronger code (polynomial [225 331 367], see [26]), also used to obtain results in Table I, the proposed SF with both long and short equalizers results in an
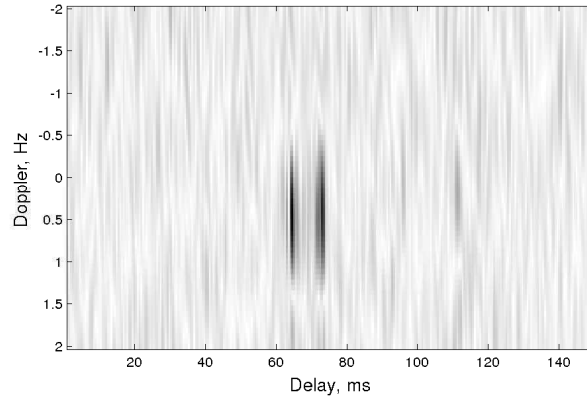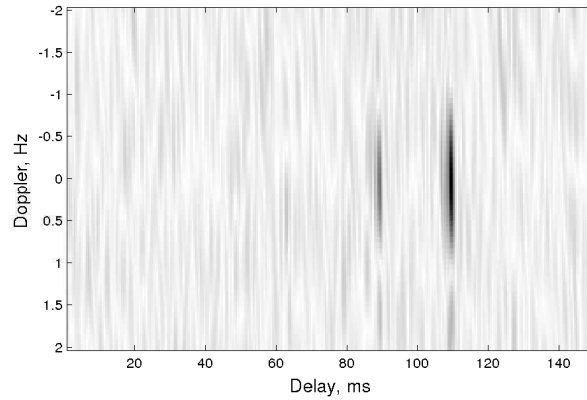
(a) Received signal at the 1st hydrophone.

(b) Directional signal at $\hat{\theta}_1 = 8.4°$.

(c) Directional signal at $\hat{\theta}_2 = -9°$.

Fig. 13. Doppler-delay spread of the signal received at the first hydrophone and directional signals in the sea trail at the distance 105 km.

error-free transmission. With weaker codes (polynomials [25 33 37] and [3 7 7]), the shorter equalizers allow a better detection performance. It is also seen that the SFs 5 and 6 show similar detection performance for the stronger codes (polynomials [25 33 37] and [225 331 367]), and SF 6 shows somewhat better performance for only the weak code (polynomial [3 7 7]).

B. Experiment at the distance 46 km

In this sea trial, $L = 120$ guard-free OFDM symbols were continuously transmitted. Space-time clusters for this sea trial are shown in Fig. 3(c). It can be seen that there are two DoAs, at $-0.2°$ and $-10.2°$, each with a single macro-path. In this

case, the beamformer is capable of separating these paths and, as can be seen below, the equalization is simplified.

1) Comparison of SFs: In this subsection, results are presented for the case when the RLS filter length in the channel estimator is set to 150 ms, which matches to the channel delay spread at a single hydrophone (as can be seen in Fig. 14), and the equalizer length is set to 500 ms. For every OFDM symbol, the transmitted data are encoded using convolutional codes with code rates 1/5 or 1/6.
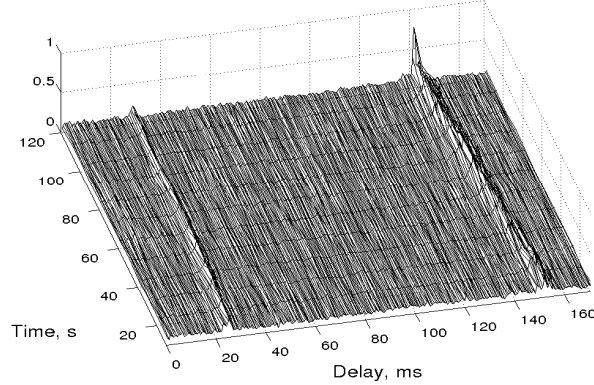

Fig. 14.   Fluctuations of the channel impulse response at the first hydrophone in the sea experiment at the distance 46 km.

Fig. 15 shows the average power $\tilde{P}(\theta)$ in this experiment. The stronger path arrives from the direction $\hat{\theta}_1 = -0.2°$, and the weaker path arrives from the direction $\hat{\theta}_2 = -10.2°$.
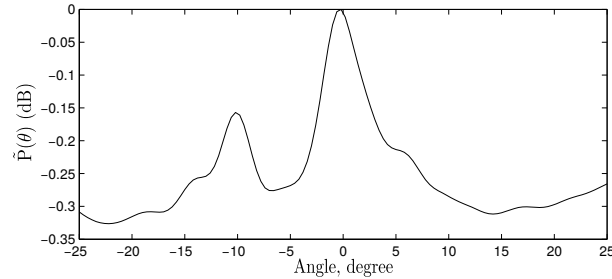

Fig. 15.   The average spatial signal power $\tilde{P}(\theta)$ at the distance 46 km.

Table III compares the BER performance for the case of code rate 1/6, which corresponds to the spectral efficiency 0.167 bps/Hz, and complexity of the receiver with different SFs. It is seen that the proposed SF 5 reduces the receiver complexity by about 5 times compared to the receiver with the SF using fractional delays (SF 6).

From Table III, it is seen that the receiver applied to a single hydrophone (SF 1) is unable to recover reliably the transmitted data. This is due to a low SNR on a single hydrophone, as shown in Fig. 16. The receiver with equalizers applied directly to all 14 antenna elements (SF 2) reduces the BER only slightly, while greatly increasing the receiver complexity. With one and two diversity branches chosen based on the maxima of the average spatial power distribution (SF 3 and SF 4, respectively), the BER performance further slightly improves. However, the difference in the BER performance for these two SFs is small, whereas the complexity of the receiver with SF 4 is almost twice compared to the SF 3. The receiver with SF 5 and SF 6 significantly reduces the BER, however, the receiver with the proposed SF 5 has about 5 times lower complexity. Thus, the

TABLE III
COMPARISON OF RECEIVERS WITH DIFFERENT SPATIAL FILTERS; SEA TRIAL AT THE DISTANCE 46 KM

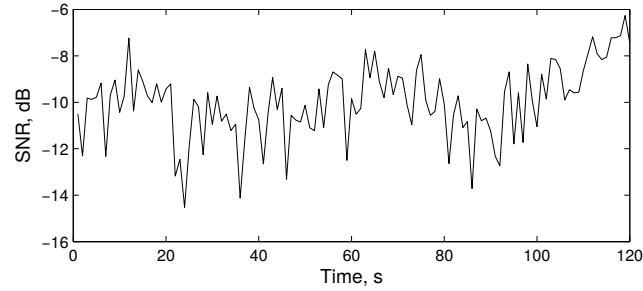| SF	Comments	BER	Complexity $(10^6$ MAC/s)
1	Single hydrophone	0.48	154
2	All 14 hydrophones	0.43	2162
3	Single angle $-0.2°$	0.11	170
4	Angles $-0.2°$ and $-0.6°$	0.09	327
5	**Cluster $(-0.2°$ and $-10.2°)$**	0	327
6	Cluster $(-0.2°$ and $-10.2°)$	0	1632

Fig. 16. SNR at the first hydrophone in the sea trial at the distance 46 km.

main conclusions on the performance of the proposed SF 5 made for the experiment at the distance 105 km also hold for the experiment at the distance 46 km.

2) Equalizer optimization: Fig. 14 shows fluctuations of the channel impulse response at the first hydrophone. The delay spread of the signal received at the first hydrophone is estimated as about 125 ms. To cover all delay fluctuations throughout the communication session, the RLS filter length is set to 150 ms; then the equalizer length is set to 500 ms. At angles $\hat{\theta}_1 = -0.2°$ and $\hat{\theta}_1 = -10.2°$, the delay spreads $d_s(\hat{\theta}_1)$ and $d_s(\hat{\theta}_2)$ of the directional signals are reduced to about 6 ms; the RLS filter lengths are set to 10 ms and the equalizer lengths are set to 35 ms.

TABLE IV
PERFORMANCE OF THE RECEIVER WITH OPTIMIZED EQUALIZERS; SEA TRIAL AT THE DISTANCE 46 KM. CODE POLYNOMIALS IN OCTAL ARE:
[37 27 33 25 35] (CODE-1); [37 35 27 33 25 35] (CODE-2); [235 253 313 331 357 375] (CODE-3). CODE RATES ARE: 1/5, 1/6, 1/6, RESPECTIVELY.

SF	Equalizer lengths	BER for code			Complexity $(10^6$ MAC/s)
		code-1 (rate 1/5)	code-2 (rate 1/6)	code-3 (rate 1/6)	
5	500 ms, 500 ms	9.6×10^{-3}	2.1×10^{-3}	0	327
5	**35 ms, 35 ms**	6.7×10^{-3}	7.0×10^{-4}	0	61
6	500 ms, 500 ms	6.9×10^{-3}	9.0×10^{-4}	0	1632
6	35 ms, 35 ms	5.0×10^{-3}	5.0×10^{-4}	0	1366

Table IV shows the BER performance and complexity of the receiver using SF 5 and SF 6, with and without adjustment of the equalizer length to the delay spread of directional signals. In the latter case, both the equalizers are of length 500 ms, whereas in the former case, they are set to 35 ms. Results in Table IV are presented for three convolutional codes with code rates 1/5 and 1/6. The stronger code (code-3) with the code rate 1/6 allows error-free transmission of this data package; this

corresponds to a spectral efficiency of 0.167 bps/Hz. It is seen that the shorter equalizers allow improvement in the detection performance and significant reduction in the complexity of the receiver with the proposed SF 5 (by about 5.4 times). This however, is not the case for the receiver with SF 6, since, in this case, the SF complexity dominates the receiver complexity. Thus, the total reduction in the complexity when using the SF 5 is about 22 times. The receiver with the proposed beamforming (SF 5) achieves the detection performance close to that of the receiver with the fractional-delay beamforming (SF 6), whereas requiring significantly lower computational load.

VI. Conclusions

In this paper, we investigated a receiver with various spatial filters for detection of OFDM signals in underwater acoustic communications. Analysis of signals recorded on a vertical linear antenna array in sea trials shows that the propagation channel is characterised by a number of space-time clusters. The use of the cluster structure of received signals in the spatial filter is shown to improve the detection performance of the receiver, compared to a multi-channel receiver with direct equalization of hydrophone signals or a receiver with directional signals generated based on the maxima of the spatial power distribution. Moreover, due to a reduced Doppler-delay spread of signals within clusters, extra performance improvement can be achieved with a reduced complexity. In this paper, we have also proposed a spatial filter that has a significantly lower complexity compared to the spatial filter with fractional delays of hydrophone signals, whereas still providing a high detection performance.

Acknowledgements

References

[1] M. Stojanovic, J. A. Catipovic, and J. G. Proakis. Reduced-complexity spatial and temporal processing of underwater acoustic communication signals. *The Journal of the Acoustical Society of America*, 98(2):961–972, 1995.

[2] Z. Xu, Y. V. Zakharov, and V. P. Kodanev. Space-time signal processing of OFDM signals in fast-varying underwater acoustic channel. In *IEEE Oceans 2007-Europe, Aberdeen, UK*, pages 1–6, 18-21 June, 2007.

[3] S. Ijaz, A. Silva, and S. M. Jesus. Arrival-based equalizer for underwater communication systems. *Conference Ucomms'12, Sestri Levante (Italy)*, Sept. 2012.

[4] A. Amar, Y. Buchris, and M. Stojanovic. Angle-of-arrival-based detection of underwater acoustic OFDM signals. In *IEEE 16th International Workshop on Signal Processing Advances in Wireless Communications (SPAWC), Stockholm, Sweden*, pages 326–330, 2015.

[5] M. Pajovic and J. C. Preisig. Performance analysis and optimal design of multichannel equalizer for underwater acoustic communications. *IEEE Journal of Oceanic Engineering*, 40(4):759–774, 2015.

[6] J. Li and Y. V. Zakharov. Space-time cluster combining for UWA communications. In *IEEE OCEANS'16, Shanghai, China*, 10–13 April, 2016.

[7] D. G. Brennan. Linear diversity combining techniques. *Proceedings of the IRE*, 47(6):1075–1102, 1959.

[8] M. Stojanovic, J. Catipovic, and J. G. Proakis. Adaptive multichannel combining and equalization for underwater acoustic communications. *The Journal of the Acoustical Society of America*, 94(3):1621–1631, 1993.

[9] Q. Wen and J. A. Ritcey. Spatial diversity equalization applied to underwater communications. *IEEE Journal of Oceanic Engineering*, 19(2):227–241, 1994.

[10] V. Capellano. Performance improvements of a 50 km acoustic transmission through adaptive equalization and spatial diversity. In *MTS/IEEE Conference Proceedings OCEANS'97.*, volume 1, pages 569–573, 1997.

[11] M. Xia, D. Rouseff, J. A. Ritcey, X. Zou, C. Polprasert, and W. Xu. Underwater acoustic communication in a highly refractive environment using SC–FDE. *IEEE Journal of Oceanic Engineering*, 39(3):491–499, 2014.

[12] M. Stojanovic, J. A. Catipovic, and J. G. Proakis. Reduced-complexity simultaneous beamforming and equalization for underwater acoustic communications. In *Proceedings of IEEE OCEANS'93. Engineering in Harmony with Ocean.*, pages III426–III431, 1993.

[13] M. Stojanovic. Recent advances in high-speed underwater acoustic communications. *IEEE Journal of Oceanic Engineering*, 21(2):125–136, 1996.

[14] L. R. LeBlanc and P. P. Beaujean. Spatio-temporal processing of coherent acoustic communication data in shallow water. *IEEE Journal of Oceanic Engineering*, 25(1):40–51, 2000.

[15] P. P. Beaujean and L. R. LeBlanc. Adaptive array processing for high-speed acoustic communication in shallow water. *IEEE Journal of Oceanic Engineering*, 29(3):807–823, 2004.

[16] L. LeBlanc. Angular-spectral decomposition beamforming for acoustic arrays. *IEEE Journal of Oceanic Engineering*, 9(1):31–39, 1984.

[17] C. He, K. Cheng, Q. Li, W. Shi, and Q. Zhan. Beam diversity for single-carrier block transmission underwater acoustic communications. In *IEEE International Conference on Signal Processing, Communications and Computing (ICSPCC)*, pages 1–5, 2016.

[18] K. T. Wong and M. D. Zoltowski. Extended-aperture underwater acoustic multisource azimuth/elevation direction-finding using uniformly but sparsely spaced vector hydrophones. *IEEE Journal of Oceanic Engineering*, 22(4):659–672, 1997.

[19] J. A. Catipovic and L. E. Freitag. High data rate acoustic telemetry for moving ROVs in a fading multipath shallow water environment. In *Proceedings of the IEEE Symposium on Autonomous Underwater Vehicle Technology, AUV'90,*, pages 296–303, 1990.

[20] J. A. Catipovic and L. E. Freitag. Spatial diversity processing for underwater acoustic telemetry. *IEEE Journal of Oceanic Engineering*, 16(1):86–97, 1991.

[21] G. Pinero and A. C. Singer. MMSE beamformer based on partial FFT demodulation for OFDM underwater acoustic communications. In *Proceedings of the 20th European Signal Processing Conference (EUSIPCO)*, pages 2308–2312. IEEE, 2012.

[22] Y. V. Zakharov and V. P. Kodanev. Experimental study of an underwater acoustic communication system with pseudonoise signals. *Journal of Acoustical Physics*, 40(9):707–715, 1994.

[23] Y. V. Zakharov and V. P. Kodanev. Multipath-Doppler diversity of OFDM signals in an underwater acoustic channel. In *Proceedings of the IEEE International Conference on Acoustics, Speech, and Signal Processing, (ICASSP), Istanbul, Turkey*, volume 5, pages 2941–2944, 2000.

[24] Y. V. Zakharov and A. K. Morozov. Adaptive sparse channel estimation for guard-free OFDM transmission in underwater acoustic channels. In *12th European Conference on Underwater Acoustics*, Corfu, Greece, June, 2013.

[25] Y. V. Zakharov and A. K. Morozov. OFDM transmission without guard interval in fast-varying underwater acoustic channels. *IEEE Journal of Oceanic Engineering*, 40(1):144–158, 2015.

[26] J. G. Proakis. Digital communications. *McGraw-Hill, New York*, 1995.

[27] B. Li, S. Zhou, M. Stojanovic, L. Freitag, and P. Willett. Multicarrier communication over underwater acoustic channels with nonuniform Doppler shifts. *IEEE Journal of Oceanic Engineering*, 33(2):198–209, 2008.

[28] S. Yerramalli and U. Mitra. On optimal resampling for OFDM signaling in doubly-selective underwater acoustic channels. In *IEEE OCEANS'2008*, pages 1–6, 2008.

[29] S. Haykin, J. H. Justice, N. L. Owsley, J. L. Yen, and A. C. Kak. *Array signal processing*. Prentice-Hall, Inc., Englewood Cliffs, NJ, 1985.

[30] J. Li, P. Stoica, and Z. Wang. On robust Capon beamforming and diagonal loading. *IEEE Transactions on Signal Processing*, 51(7):1702–1715, 2003.

[31] H. Krim and M. Viberg. Two decades of array signal processing research: the parametric approach. *IEEE Signal Processing Magazine*, 13(4):67–94, 1996.

[32] K. Tu, D. Fertonani, T. M. Duman, M. Stojanovic, J. G. Proakis, and P. Hursky. Mitigation of intercarrier interference for OFDM over time-varying underwater acoustic channels. *IEEE Journal of Oceanic Engineering*, 36(2):156–171, 2011.

[33] A. Radosevic, R. Ahmed, T. M. Duman, J. G. Proakis, and M. Stojanovic. Adaptive OFDM modulation for underwater acoustic communications: Design considerations and experimental results. *IEEE Journal of Oceanic Engineering*, 39(2):357–370, 2014.

[34] K. Tu, T. M. Duman, M. Stojanovic, and J. G. Proakis. Multiple-resampling receiver design for OFDM over Doppler-distorted underwater acoustic channels. *IEEE Journal of Oceanic Engineering*, 38(2):333–346, 2013.

[35] S. F. Mason, C. R. Berger, S. Zhou, and P. Willett. Detection, synchronization, and Doppler scale estimation with multicarrier waveforms in underwater acoustic communication. *IEEE Journal on Selected Areas in Communications*, 26(9):1638–1649, 2008.

[36] C. H. Yuen and B. Farhang-Boroujeny. Doppler scaling correction in OFDM. In *IEEE International Conference on Communications (ICC)*, pages 4713–4717, 2013.

[37] C. H. Yuen and B. Farhang-Boroujeny. Non-linear Doppler scaling correction in underwater acoustic channels: Analysis and simulation. In *2013 IEEE OCEANS-San Diego*, pages 1–7, 2013.

[38] B. S. Sharif, J. Neasham, O. R. Hinton, and A. E. Adams. A computationally efficient Doppler compensation system for underwater acoustic communications. *IEEE Journal of Oceanic Engineering*, 25(1):52–61, 2000.

[39] T. H. Eggen, A. B. Baggeroer, and J. C. Preisig. Communication over Doppler spread channels. Part I: Channel and receiver presentation. *IEEE Journal of Oceanic Engineering*, 25(1):62–71, 2000.

[40] J. Li and Y. V. Zakharov. Sliding window adaptive filter with diagonal loading for estimation of sparse UWA channels. In *IEEE OCEANS'16, Shanghai, China*, 10–13 April, 2016.

Jianghui Li received his B.S. degree in Communications Engineering from Huazhong University of Science and Technology, Wuhan, China in 2011. From 2011 to 2012, he was with Chinese Academy of Sciences as a research assistant. He received his M.Sc. degree in Communications Engineering in 2013 from University of York, U.K., where he is currently working towards the Ph.D. degree in Communications Engineering with the Department of Electronics.

His research interests include wireless communication networks, underwater acoustic communications, adaptive signal processing and array beamforming.

Yuriy V. Zakharov received the M.Sc. and Ph.D. degrees in electrical engineering from the Power Engineering Institute, Moscow, Russia, in 1977 and 1983, respectively.

From 1977 to 1983, he was with the Special Design Agency in the Moscow Power Engineering Institute. From 1983 to 1999, he was with the N. N. Andreev Acoustics Institute, Moscow. From 1994 to 1999, he was with Nortel as a DSP Group Leader. Since 1999, he has been with the Communications Research Group, University of York, U.K., where he is currently a Reader in the Department of Electronics. His research interests include signal processing, communications, and acoustics.